Heat and Mass Transfer, Vol. 54, Issue 1, January 2018, pp. 209-226
DOI:10.1007/s00231-017-2118-0

Void fraction development in gas-liquid flow after a U-bend in a vertically upwards serpentine-configuration large-diameter pipe

Almabrok A. Almabrok[a], Aliyu M. Aliyu[b*], Yahaya D. Baba[c], Liyun Lao[d], Hoi Yeung[d]

[a]Department of Petroleum Engineering, Faculty of Engineering, Sirte University, Sirte, Libya

[b] School of Mechanical Engineering, Pusan National University, 609-735, Busan, Republic of Korea

[c] Chemical/Petroleum Engineering Department, Afe Babalola University, PMB 5454, Nigeria

[d]Oil and Gas Engineering Centre, School of Water, Energy and Environment, Cranfield University, Bedfordshire MK43 0AL, United Kingdom

*Corresponding author email: aliyu@pusan.ac.kr (A M Aliyu)
Tel: +82-51-510-3441

Abstract

We investigate the effect of a return U-bend on flow behaviour in the vertical upward section of a large-diameter pipe. A wire mesh sensor was employed to study the void fraction distributions at axial distances of 5, 28 and 47 pipe diameters after the upstream bottom bend. It was found that, the bottom bend has considerable impacts on up-flow behaviours. In all conditions, contour plots of the cross-sectional phase distribution measurement using the wire mesh sensor (WMS) show that centrifugal effect of the U-bend causes appreciable misdistribution in the adjacent straight section. However, flow asymmetry significantly reduces at an axial distance of 47D from the U-bend. Flow regime maps generated from three axial locations showed that, in addition to bubbly, intermittent and annular flows, oscillatory flow occurred particularly when gas and liquid flow rates were relatively low. At this position, the mean void fractions were in agreement with those from other large-pipe studies. Comparisons were made with existing void fraction correlations. Among the correlations surveyed, drift flux-type correlations were found to give the best predictive results.

Keywords: *pipe bends, multiphase flow, two-phase flow, void fraction distribution, wire mesh sensor.*

Nomenclature

A. Roman		
C_o	[-]	Distribution parameter
D	[m]	Pipe internal diameter
Fr	[-]	Froude number
g	[m/s^2]	Acceleration due to gravity
G	[kg/m^2-s]	Total liquid mass flux
L	[m]	Pipe length
P	[Pa]	Local pressure
Re	[-]	Reynolds number
S	[-]	Slip ratio
u	[m/s]	Phase velocity as specified by subscript
U^+	[-]	Dimensionless velocity
We	[-]	Weber number
x	[-]	Gas quality
y^+	[-]	Friction distance parameter
B. Greek		
Δ	[-]	Operator denoting change in the variable that follows
ε	[-]	Void fraction
μ	[kg/s-m]	Dynamic viscosity
ρ	[kg/m^3]	Density
σ	[N/m]	Liquid surface tension
C. Subscripts		
g	Gas phase	
h	homogenous	
l	Liquid phase	
mix	Mixture	
lf	Liquid film	
sg	Superficial gas	
sl	Superficial liquid	

1 Introduction

1.1 Background

Gas–liquid flows in pipelines with a serpentine shape are frequently encountered in heat exchangers and transport pipes used in a variety of industries such as nuclear, process and oil and gas. In the oil and gas sector, it is usual that transport pipes for the processing of wet gases have a serpentine configuration. Therefore, around the bends (which could be up to 180°), large centrifugal forces are generated and these cause substantial flow misdistribution such that local dry spots are created. In cases where heat transfer is involved, dryout or critical heat flux can occur. This may cause costly shutdown/unscheduled maintenance of facilities ultimately leading to increased operating costs. It is therefore necessary to have comprehensive knowledge of bend effects on the flow downstream of the bend. This is needed for the safe and efficient design and operation of pipelines for gas–liquid transport in the offshore oil and gas sectors.

Significant amounts of studies are available in the literature on two-phase flow in bends. The majority of them focus on upward flow with small diameter pipes ranging from 25 to 50 mm. However, the studies of the upward flows with large-diameter pipes (larger than 100 mm), are increasingly considered in recent years as problems related to large-diameter vertical pipes become more frequently encountered in industry. The current work intends to study the effect of 180° bends in a 4-inch (101.6 mm) internal diameter pipe by investigating the characteristics and development of gas-liquid two-phase flow using a capacitance Wire Mesh Sensor (WMS).

A number of researchers [1]–[4] examined the influence of return bends on flow patterns. Specifically, Oshinowo and Charles [2] utilised conductance sensors to measure flow distribution. In their analysis, they considered a force balance between centrifugal and gravitational forces acting on the phases in the bend to qualitative discuss a modified Froude number, which was related to the mean cross-sectional void fraction in the bend.

Takemura et al. [5] conducted an experimental study on the characteristics of dryout and pressure drops in air–water flows in a U- as well as an inverted 180° U-bend of 18-mm internal diameter. From their data, they remarked that the flow behaviour of the respective geometries were different within the bend. The gas flowed on the inner surface of the U-bend in all the flow conditions tested. They observed that the prevalence of dryout is higher in the case of a U-bend than in the inverted U-bend.

Poulson [6] investigated mass transfer in return bends and stated that when compared to the straight section mass transfer is higher as superficial gas velocity increases. In contrast, it is constant at low superficial liquid velocities. An experimental study was done on liquid drop size in horizontal to 90° bend in annular flows by Ribero et al. [7]. They used a 32-mm pipe facility and they produced a droplet size distribution within the bends, which they noted was different from those in straight sections. [8] developed a pressure loss correlation over 90° bends in terms of the Martinelli two-phase flow

multiplier. The correlation was derived using pressure loss measurements in vertical 90° bends with 30-mm diameter and curvature radii of 120, 180, 240 and 300 mm and they showed that is well predicts their data as well as others to within ±20%.

Other studies on bends are also available in the literature for slightly larger pipelines. Hoang and Davis [9] studied void fraction in froth flow in a 50-mm U-bend by utilising conductance needle probes. James et al. [10] investigated droplet behaviour in a 90° horizontal elbow with 67.4 mm diameter while Chong et al. [11] derived a model for vertical tubes connected by 180º bends. This was an extension of the phenomenological model for annular flow in a single vertical channel proposed by Azzopardi [12]. The model predicted dryout in serpentine geometry fired-channel reboilers for hydrocarbon processing. This model was found to sufficiently confirm the decrease of film flow rate to zero before the last bend as previously predicted by Balfour and Pearce [13] for C-shaped bends. Others include the study by Domanski and Hermes [14] on an improved pressure drop correlation in a 180° return bend for refrigerants R-22 and R-410A in 3 and 12 mm pipes. Sharma et al [15] also conducted a study on 180° U-shaped and rectangular-shaped pipes of 12 mm internal diameter. However, their study considered co-flow of oil and water. It is important to note that all the aforementioned are in small diameter pipes of internal diameter less than 100 mm.

Reported literature on two-phase air-water flow in 180º bends in large-diameter pipes is scarce. Large diameter pipes are defined as those with internal diameter greater than 100 mm. The only one we were able to find were those by Oshinowo and Charles [2] and Abdulkadir et al. [16]. They conducted air–water experiments in a vertical 180º bend with 127 mm pipe diameter within the churn-annular flow regime. A conductance tomography sensor was used to measure mean film fraction before, within, and after the bend. They observed that conditions for which the liquid goes inside or outside of the bend can be identified using the values of Froude number modified based on the work of Hills [17].

The literature survey above suggests that bends have a considerable effect on gas–liquid flow characteristics in the straight sections downstream of the bend, and how far this propagates has not been thoroughly investigated previously. More so, earlier studies were mainly confined to small diameters with the majority carried out in pipes with internal diameter less than 50 mm. Thus, there is still a need for studies and data on two-phase flows in large-diameter pipes. This is particularly important as other authors [18]–[23], have shown that the gas-liquid flow behaviour in large-diameter pipes differs from those in smaller size pipes.

We present further experimental data on two-phase flow behaviours in a serpentine configuration pipe in order to aid in understanding and improve design capability. Particularly, we highlight the effects of 180° bend on gas void fraction distributions in the upward vertical section, as gas void is very vital for identifying the operating conditions in which dryout or critical heat flux should be avoided.

1.2 Void fraction correlations and data

One variable that is critical in predicting pressure drops and heat transfer in pipes is the cross-sectional void fraction, which is the portion of pipe occupied by the gas. Usually, numerical solutions of the two- or three-field model can be obtained to simultaneously predict the void fraction and pressure drop, but the accuracy of this approach is reliant on and very sensitive to the choice of interfacial/wall friction factor correlations ([24] and [25]). Therefore, a layer of uncertainty is introduced in the calculations for the void fraction/pressure drop using the two- or three-field models.

Engineers hence resort to the use of empirical correlations for void fraction prediction and many have been developed over the years. However, choosing a suitable correlation for a certain set of flow regimes, pressure range, fluid properties and pipe geometry is indeed a daunting task. Apart from the fact that most of the correlations have one of form of restriction or another accompanying their application, discontinuities can occur when transferring from one correlation to another for different practical operating conditions [26]. One way these discontinuities can occur is the use of a correlation outside the range of fluid properties, test conditions, or pipe diameter from which the underlying data was obtained. As stated earlier, pipe diameter alone, and by extension, scalability of correlations one is a major factor affecting their accuracy. While most of the correlations in the literature were obtained from small pipes (mostly 50 mm diameter and below), industrial pipes in the oil and gas or nuclear industries are generally greater than 100 mm in diameter. Nevertheless, predictive correlations for large pipe void fractions are scarce and only few are available in the literature [18], and [27]. These are drift flux-type correlations of the form:

$$\varepsilon = \frac{u_{sg}}{\left(C_o u_{mix} + U_{gj}\right)} \tag{1}$$

where C_o isthe distribution parameter and U_{gj} is the drift velocity. Relationships for them are obtained empirically and are flow-regime dependent. For these correlations and their application ranges, relationships were developed for C_o and U_{gj}^{+}. Comparison with various experimental data showed that the former model was only suitable for application at low mixture volumetric flux; while the latter agreed better at higher mixture volumetric fluxes where spherical cap bubbly, churn, and annular flows occur. Drift flux correlations give good agreement with large databases consisting of pipes with diameters between 10 and 600 mm and are accurate to within ±20%. They are phenomenological or flow regime dependent meaning that flow regime transition criteria need to be applied and these are dependent on pipe size, system pressure, and flow direction (upwards, downwards, or inclined). Additionally, in flow codes, this could introduce extra layers of complication within iterations potentially slowing down simulations. That is why investigators continue to develop simpler drift flux-type correlations for certain ranges of system pressures and pipe diameters, as well as correlations based on the homogeneous model, and those based on the slip ratio irrespective of flow regime. As summarised in Table 1, seven of the most frequently used in the open literature have been gathered. These were developed using experimental measurements in pipes mostly of diameter below 50 mm.

Woldesemayat and Ghajar [26] compared many of these correlations against an experimental database comprising the experiments of previous investigators which were also mostly carried out using small-diameter pipes. This does not tell us how well the correlations will perform against larger channel two-phase flow. In order to make such an evaluation, we have gathered an experimental databank (Table 2) of purely large pipe data of low-high gas flow from bubbly to annular flow. The databank consists of the current measurements in a 101.6 mm vertical pipe system (reported in previous sections); as well as the measurements of Zangana [28] and Van der Meulen [29] in 127 mm diameter flow loops at the University of Nottingham; and Skopich et al. [30] in a 101.6 mm vertical pipe at the University of Tulsa, Oklahoma.

Table 1: Selected void fraction correlations

Table 2: Sources of void fraction data for large-diameter upward flow

2 Experimental setup

2.1 Test facility

The test facility, located in the PSE Laboratory at Cranfield University, comprises of three sections namely the fluid supply and metering section; test section; and the phase separation section. Figure 1 shows the schematic of a purpose-built rig, the Serpent test facility used for this study.

- **Fluid supply and metering section**

Air is supplied from a bank of two compressors GA75 and GA55, and these can deliver air for tests at a flow rate up to 2000 Sm^3/h. The air from the compressors first accumulates in an 8-m^3 air receiver to damp pressure fluctuations from the compressor. The air then passes through a series of three filters and then through a cooler where debris and moisture stripping occurs before metering. Airflow control is achieved using two control valves connected to an Emerson DeltaV plant management system. One of two Rosemount Mass Probar flow meters FA1 and FA2 depending on the airflow rate range does the metering, and the pneumatic actuators connected to the DeltaV system automatically control this. Water is supplied from a 1.2-m^3-water tank to the flow loop by a Grundfos CRE3 26-speed variable pump, with a maximum duty of 10 L/s at 6 bar pressure. Hence, the pump and compressors are capable of providing the required flow rates of the current experiments (air: maximum of 1200 Sm3/h, water: 8 L/s) without pulsation. Water flow rate is regulated by adjusting the pump speed, and/or operating the manual bypass valve VW2 between the outlet of the pump and water tank. The water flow rate is measured using a 100-mm ABB electromagnetic flow meter. The air and water are mixed at a T-joint before entering the test section.

- **Test section**

The test section consists of the flow rig, which has a length of about 20.0 m. The internal diameter is 101.6 mm and this comprises of four vertical sections connected by two 180° return bends which have wall roughness estimated at around 5×10^{-6} m. The bends have a radius of 203 mm and were precision-made from Perspex blocks. The two 6-m long downward and upward vertical legs are the test sections and each has three measurement and observation stations located at different positions along the pipe. In each measurement position is a liquid film sensor assembly consisting of four sensor probes, used to measure liquid film thickness, and a spool for the WMS. This spool is usually placed downstream of the liquid film sensor spool so that its intrusiveness has no effect on the film thickness probes. Six GE PMP4070 pressure transducers, P1-P6, are also installed for measuring the pressure drops along pipe sections. Finally, two temperature sensors, PT1 and PT2 are installed at the entrance and exit locations of the pipeline. These are frequently recalibrated due to ambient temperature shifts that can occur from time to time.

- **Phase separation section**

This section consists a vented covered tank where air is separated from the water and vented. The water flows by gravity back to the storage tank via a 150-mm pipe. This is recirculated to the flow loop using the Grundfos variable-speed pump. Filters have been installed throughout the flow loop to reduce debris circulation to the barest minimum and these are frequently changed. A manual ball valve between the test section and the ventilation tank was installed for regular leakage checks, pressure adjustment and testing. All straight sections in the test facility are made from ABS plastic. The test facility is rated at 10-bar pressure at ambient temperature conditions.

Figure 1: Schematic of the Serpent rig. Location of WMS is at MV21, MV22 and MV23 corresponding to L/D = 5, 28 and 47 respectively.

2.2 Installed instruments

A capacitance Wire Mesh Sensor (WMS) was installed at various locations of the straight sections to obtain cross-sectional phase distribution. As shown in Figure 2, the WMS has wire electrodes, which have been stretched across the flow cross-section. The two sets of wire electrodes are perpendicular to each other and separated by a distance of 2.5 mm. One set acts as the sender while the other acts as the receiver. The spacing between two parallel wires is 3.2 mm. A sampling rate of 1000 fps is used for data acquisition. The electrodes of the sender are activated when excitation current is passsed in a sequence while the receiver electrodes are parallel sampled. The WMS measuring principle is based on local conductivity or permittivity changes between the gaps of each crossing point. By sequentially applying an excitation voltage to each sender electrode while the others are at kept at ground potential, the current flow to receiver electrodes can be measured and related to the phase

fractions present. Further details and reading can be done on the WMS design and principle of operation in [31].

Figure 2 is a picture of the WMS used and a schematic illustrating the nomenclature of the wires connecting to the sender electronics, which are in the 0° –180° direction, and the wires connecting to the receiver are in the 90°–270° direction. This arrangement allows for the chordal distribution of the void fraction along both angular directions to be appropriately obtained from the cross-sectional distribution of the void fraction.

Figure 2: (a) WMS (b) its cross-sectional orientation (c) validation of WMS void fraction with those obtained by ΔP and film thickness (FT) measurements at $u_{sl} = 0.2$ m/s

On the straight upwards section of the Serpent rig, void fraction measurements by other methods were compared with the time and cross-sectionally averaged void fraction values obtained from the WMS. The upwards section was chosen as the regimes in this section cover a wide range of vertical flow regimes as the gas flow rate is increased. In the validation tests, a low liquid superficial velocity of 0.1 m/s was used, while the air velocity varied in the range of 0.15–10.00 m/s. In these conditions, interfacial friction forces are small and the pressure drop is dominated by the gravitational component. Therefore, in the momentum balance equation, the frictional component is negligible and the void fraction can be easily obtained from the differential pressure P using the pressure transducers P4 and P5. These give values that can be used for the validation of the WMS values measured near the visual observation station MV22, which is the middle point between the locations of pressure transducers P4 and P5 on the pipe. The distance L between the two transducers is 4.1 m. Since the frictional pressure drop can be neglected as earlier discussed, ε, i.e. the mean cross-sectional void fraction by the WMS can be calculated as follows:

$$\varepsilon = 1 - \frac{\Delta P/L}{g(\rho_L - \rho_g)} \tag{2}$$

where $\Delta P/L$ is the pressure gradient between the two transducers P4 and P5. The instruments in the Serpent rig also include air and water flow meters, pressure sensors, and temperature sensors. Figure 2c shows that deviations between the measured void fractions between the WMS and ΔP methods are within ±15% deviation from each other. The largest deviations are apparent at the higher void values and these occur because as the gas void fraction becomes higher, especially when the flow pattern is annular, frictional forces become more and more dominant and these cannot be ignored. For such conditions, it was much easier to validate WMS readings with film thickness (FT) measurements, and this was done using flush-mounted conductance probes, of which details have been previously published [32], [33]. Void fraction can be calculated from FT assuming negligible droplet entrainment

occurs by dividing the void area by the total pipe area. After simplification, the relationship is as follows:

$$\varepsilon = \left(\frac{D - 2t}{D}\right)^2 \tag{3}$$

where D is the pipe diameter and t is the liquid film thickness, mean of four probes. The conductance probes have a measuring uncertainty of ±3%, and as can be seen from Figure 2 (c), good agreement exists between their void fraction values and that obtained by the WMS. However, all the void fractions estimated using the FT measurements produced slight overpredictions which are due to the presence of small quantities of entrained droplets in the core area, but which Equation (3) ignores. Nevertheless, the WMS and FT void fractions are well within +5% of each other. The manufacturers originally calibrated the air and water flow meters, but to ensure their accuracy, we also checked them by cross-calibrating using other flow meters in the laboratory. The quick closing valve method was also used to verify the values for the water flow meters. The pressure sensors were also checked in situ using a portable pressure tester to ensure deviations of less than ±1% from calibrated values, otherwise, they get recalibrated.

3 Results and discussion

3.1 Flow regime identification

We investigated flow regime development along the upward flowing pipe straight by examining the data of cross-sectional phase distributions. Figure 3 illustrates the axial slice images in the X– and Y–axes respectively and cross-sectional images in the Z-direction of the gas–liquid mixture at the bottom, middle and top positions of the upward flowing section. The images were reconstructed from the WMS data at different ranges of superficial air velocities u_{sg}, and for a fixed superficial water velocity u_{sl} of 1 m/s. Each image in the X-direction was obtained by stacking axially sliced cross-sectional images along the 0°–180° direction (refer to Figure 2 (b) for the definition of the angular directions). Similarly, for images along 90°–270° direction, the cross-sectional image numbers used to reconstruct the axial slice images is inversely proportional to the mixture velocity U_{mix}, in order to give near-reality phase structures inside the pipe. The number *N* of slices required to reconstruct a certain length of pipe is expressed as, $N = f_s L_p / U_{mix}$, where f_s is the recording frame rate (1000 fps here); L_p is the perceived length of pipe section represented by the axial sliced images, i.e. 1000 mm in this study. Hence, the difference in time between the bottom of a reconstructed image to the top is calculated as L_p/U_{mix}. In Figure 3, the time range at the top represents this temporal perception of the images.

It was observed that the flow is bubbly for the flow condition of u_{sg} = 0.17 m/s and u_{sl} = 1 m/s (also shown in Figure 3). Characteristic of this regime are the dispersed large bubbles evenly distributed across the pipe. Transition from bubbly to intermittent flow occurs at a higher u_{sg} of 0.52

m/s. As u_{sg} increases to 1.02 m/s, these bubbles coalesce and the flow transitions to intermittent flow. Increasing u_{sg} further to 2.67 m/s also gives intermittent flow but the bubbles become larger occupying most parts of the pipe cross-section. However, annular flow regime forms on increasing u_{sg} to 18.56 m/s. At this condition, it we noted that at the bottom and middle positions, a large amount of the liquid wisps and droplets were entrained in the pipe core.

For the flow condition where u_{sg} = 1.02 m/s and u_{sl} = 1.00 m/s, large air bubbles similar to Taylor bubbles formed in the middle and top positions of the pipe. The presence of Taylor bubbles is an indication of the slug flow regime that occurs in small diameter pipes, but in this case, the bubbles do not occupy the entire pipe cross-section. In large-diameter, upward pipes there seems to the existence of a limit on the size of bubbles. It was pointed out that, this limit is due to the Raleigh–Taylor instability that prevents bubble growth with pipe size [23]. A number of authors [23], [34], [35] have observed and documented this lack of traditional Taylor bubble occurrence in large pipes.

Figure 3: Reconstructed images of the phase distributions at different locations along the upward section for different u_{sg} and a fixed u_{sl} of 1 m/s (X and Y represent the axial slice images, and Z represents cross-sectional images). Red and blue colours denote the gas and liquid phases respectively

Figure 4 presents a comparison of time traces and void fraction PDFs at the bottom, middle and top positions in the upward section at different gas flow conditions at u_{sl} = 1 m/s. The time trace data for the three positions show that at u_{sg} = 0.17 m/s, the flow regime can be classified as bubbly. The PDFs of the void fraction values at these velocities also show that the observed flow regime for the three positions as bubbly. The shapes of the PDFs are similar for all positions; however, the peak is noted to be a little higher at the top position than those at middle and bottom positions, suggesting increase in the size of bubble due to gas expansion towards the top of the pipe. For other gas flow conditions, similar PDF shapes occur at the top and middle positions and these increasingly suggest highly developed flow beginning to occur from the middle position at L/D = 28.

For air superficial velocity of 0.52 m/s, and fixed water velocity of 1 m/s, the time traces data of void fraction show similar tendencies at all locations along upward section. However, it can be noted from Figure 4 that, the height of PDF obtained at the bottom location is about 0.045, while the height of those obtained at the middle and top locations are 0.06. Figure 4 also shows that, the transition from bubbly to intermittent flows occurred at all locations of upward flow. The flow pattern identified at the bottom position is characterised by a large base of void fraction values extending from 0 to 0.6. This is because of the large size of bubbles that were created under these velocities. The time trace data obtained at the top and middle locations suggest that slug-like flow is formed when air velocity increases to 1.02 m/s evidenced by the bimodal PDFs representing the large Taylor bubbles and the smaller

trailing bubbles. The PDF at the lower pipe location gave a single peak characterised by values of gas void fraction spanning from 0.1 to 0.6 indicating good mixing between phases due to turbulence caused by the bend. When air velocity increases to 2.67 m/s, an intermittent flow with similar time traces and PDFs shapes at the top and middle locations, accompanied by huge fluctuations in void fraction. This indicates churning and the flow is in a transient (or unstable) state. Finally, at the highest gas flow rates investigated, i.e. 18.57 m/s, the single high-void fraction PDF peak is distinctive of annular flow. This condition is characterised by the liquid pushed to the pipe wall and the core is occupied by the gas flow laden with liquid droplets (See Figure 3).

Figure 4: Void fraction time traces and their PDFs at the top, middle and bottom positions at u_{sl} = 1 m/s

- **Flow regime maps**

Figure 5 shows the vertical upward flow regime maps for this study obtained using visual observation and with the aid of WMS reconstructions, videos, and shapes of void fraction PDFs at the three axial positions. Bubbly, unstable, intermittent and annular flow regimes was observed at different locations along the upward section. The classification of the above-mentioned flow regimes is related to a specific range of gas and liquid superficial velocities. Good agreement exists between the observed intermittent to annular transition boundaries at all three positions as well as the region described as unstable. On the other hand, the flow regime map obtained at the bottom position is different with respect to the bubbly to unstable flow transition in that there is a shrinking of the intermittent flow region. It can be identified from the map produced at the lower station that, the boundaries between bubbly to intermittent flows are extended to higher gas and lower liquid flow rates, as shown in Figure 5 (c). This could be due to the lower hydraulic head at the bottom position which the flow struggles to achieve on reaching the middle section leading to flow intermittence. This could also be due in part to expansion along the pipe due pressure losses. Indeed, Golan and Stenning [22] noted that in this kind of pipeline, the lower bends can be periodically blocked by liquid and, then blown through by the accumulated air. Such a behaviour is undesirable in heat exchange facilities, operating at and such conditions can be avoided using flow maps such as the current ones as guide.

It can be noted from the presented maps that, bubbly, unstable intermittent and annular flows are clearly formed at particular ranges of gas and liquid flow rates. The produced maps showed that, an intermittent flow is dominant at all locations along the upward section. This observation was supported by Azzopardi and Wren [36] who observed that churn flow is a dominant flow regime in large diameter pipes for most conditions of gas and liquid flow rates.

Figure 5: Flow regime maps at the top, middle and bottom positions of upward section, respectively of this study compared with the up-flow regime map reported by Taitel et al. [37] **(red lines and text) in 51 mm pipe diameter.**

Superimposition of the Taitel et al. [37] flow regime map on our regime observations are shown with the red lines and text in Figure 5. Their flow map was produced using different physical models for regime transitions and there is reasonable agreement between the two only in the bubbly flow region and the transition from bubbly to intermittent flow boundaries. However, the transition boundaries between intermittent (which includes churn) and annular flow are somewhat different in both studies. It can be seen that, the air velocities needed to create annular flow regime in current study (i.d. 101.6 mm diameter pipe) appear lower than those predicted by Taitel et al's map (i.d. 51 mm diameter pipe). This may partly be because flow regime transitions are not sharp but are within a range of velocities, and that hydrodynamic instabilities of churning are not sustained up to large gas flows in large diameter pipes [27], [38] and the flow quickly transits to annular flow.

3.2 Void fraction development

In Figure 6 (a-c) are the time-averaged void fractions measured using the WMS at the top, middle and bottom positions, respectively. In all the plots, there exists an asymptotic void fraction tendency with gas superficial velocity at the axial positions. The same observation was made by Abdulkadir [39] who claimed that the void fraction increases at lower superficial gas velocities sharper than that at higher superficial gas velocities. As such, the void fraction becomes less sensitive to gas flow increases at higher air flow rates than that at lower air flow rates. Conversely, void fraction values decrease as superficial liquid velocity increases which is physically consistent. It can hence be inferred that void fraction is well correlated with gas and liquid velocities when they are expressed in dimensionless form.

Figure 6: Effect of u_{sg} and u_{sl} on void fraction development at three positions of upward section (P = 0.9–1.3 bar)

Figure 7 shows plots of the void fraction ratio versus the axial distance along the upward section. We define the void fraction ratio as the ratio of the void fraction value at other positions to that at the top position (i.e. at 47 pipe diameters). Subsequently, the void fraction ratio at the top position is unity. The plots show that the void fraction variation against axial position is significantly different at lower superficial velocities (for instance at u_{sg} = 0.14 m/s and u_{sl} = 0.07 m/s) than that at higher superficial air velocities. This variation decreases with u_{sg} suggesting high gas flows have a stabilising

effect on flow development and is expected since the flow is in the direction of buoyancy. On the other hand, void fraction behaviour does not exhibit significant change when the superficial liquid velocity is changed. This suggests that gas flow is a more dominant factor on void fraction/flow development than liquid flow.

Figure 7: Void fraction variations along upward section

Figure 8 presents the chordal as well as cross-sectional phase distributions as contour plots at u_{sl} = 1 m/s for the three axial positions. The figure shows flow at u_{sg} = 0.17, 0.52, and 9.65 m/s. For the chordal plots, green indicates void fraction at the direction of wires located at 90º–270º while blue indicates those at 0º–180º directions respectively. The chordal distributions show core peaking void fractions at all axial positions as the values gradually increased towards the pipe centre. Significantly, different chordal profiles exist at the bottom when compared with those at the higher positions. While the void fraction asymmetry at the bottom is because of the flow misdistribution caused by the bend, axisymmetric profiles that occur at the higher positions suggest highly developed flow. On the other hand, flow misdistribution seems to be more pronounced along one plane (i.e. 90º–270º) rather than a three-dimensional phenomenon, and this may have contributed to the fast development on getting to L/D = 28 as observed.

The bend's impact on the flow behaviour at the bottom position becomes less as the u_{sg} increases from 0.17 to 0.52 m/s. The flow at u_{sg} = 0.52 m/s is more uniformly distributed than that for u_{sg} = 0.17 m/s along 90°–270° direction. This is more so at u_{sg} = 9.65 m/s where the flow distribution at the bottom position became more even along 90°–270° plane, further confirming earlier observations that higher gas flow enhances uniform phase distributions hence promoting flow development. Again, the bend impact is scarcely distinguishable at the middle and top positions and the flow become more evenly distributed.

Figure 8: Chordal distributions of the void fraction at the top, middle and bottom positions of upward section, for different superficial air velocities (u_{sg}) and a fixed superficial water velocity (u_{sl}) of 1.0 m/s.

3.3 Effect of pipe diameter on void fraction correlations

Among other factors such as fluid properties, flow direction, and pipe inclination, pipe diameter has one of the dominant effects on two-phase flow behaviour. Depending on pipe size, flow regimes and their transitions will be affected and these will influence the choice of appropriate

phenomenological models required for predicting flow behaviour. For example, design for slug flow may be unnecessary using pipes of large-diameter (defined as those with a diameter greater than 100 mm) since it does not occur in such pipes [23], [40]. As a result, pipe diameter can be an important factor in downstream equipment design including safety considerations.

Figure 9 shows comparisons between the experimental void fractions and the predicted values using slip ratio-type correlations. This class of void fraction correlations is in the form:

$$\varepsilon = \frac{u_{sg}}{u_{sl} + Su_{sl}} = \frac{\rho_l x}{\rho_l x + S\rho_g(1-x)} \tag{4}$$

where *x* is the gas or vapour quality and S is the slip ratio being the ratio of the gas phase to liquid phase velocity. Normally, the slip ratio is correlated with dimensionless numbers such as the density and viscosity ratios. Among the four surveyed in this category of correlations, two [41], [42] gave the better predictions with the latter being the best despite consistent under-predictions across flow regimes except for the data in annular flow where the predictions exactly match the correlation in most cases. The reason could be that for flow regimes where phase velocities are similar such as bubbly, the slip ratio is near unity; hence, a slip ratio correlation approximates a homogeneous model void fraction correlation. Turner and Wallis [43] correlated their void fraction in the fashion of Lockhart–Martinelli, maintaining the same parameters but slightly adjusting their indices to fit their experimental data. However, the void fraction appears very sensitive to the values of the indices for the particular set of dimensionless numbers.

Figure 9: Comparison of large-diameter void fractions with published slip ratio-type correlations

Figure 10 shows experimental data compared with no-slip-type void fraction models. The simplest no-slip correlation is the homogeneous model where the slip ratio in Equation (4) is unity if both phases are assumed to travel at the same velocity. This now becomes:

$$\varepsilon_h = \frac{\rho_l x}{\rho_l x + \rho_g(1-x)} = \frac{u_{sg}}{u_{mix}} \tag{5}$$

As shown in Figure 10 (a), the homogeneous performs quite well in predicting the large pipe void fractions. The highest deviations occur at the lower void fractions where many of the points were under-predicted and lie outside the -30% error line. However, there is progressive improvement as the void fraction increases such that above 0.7, only a handful of points lie outside the -30% margin. The other correlations considered in this category all largely produced under-predictions also in a similar fashion as the homogeneous model. While many of their data points lie within the specified error margin, only one (i.e. Bankoff's [44] correlation) had the majority of points outside ±30% line. This could be because

Bankoff only used only steam–water mixtures and at rather low void fractions. Overall, the non-slip void fraction correlations exhibit good performance against the large pipe two-phase measurements.

Figure 10: Comparison of large-diameter void fractions with published no-slip-type correlations

The drift-flux model has been described as one of the most accurate for gas-liquid void fraction prediction in up-flows and has been extensively applied in thermal-hydraulic codes such as TRAC-PIA and ATHOS-3 [27]. It was initially developed to account for the velocity of a large bubble relative to the mixture velocity was taken into consideration [45], [46]. The two important parameters here are the distribution parameter and the drift velocity and many authors have derived expressions for them. While the former has values that range between 1.1 and 1.3 depending on the flow regime, the latter is usually expressed as a Froude number based on the gas drift velocity. Experimentally, for bubbly flows, the drift velocity is around 0.5. However, use of the drift-flux model has expanded over the years to other flow regimes. For example several constitutive relationships were derived for the drift velocity and distribution parameter for churn–turbulent and annular flows [18]. Since in annular flow, the assumption of velocity equality between the phases can be made for thin films, the drift velocity is zero. This then makes the drift-flux void fraction in annular flow equal to a multiple of the homogeneous void fraction, the multiple being the inverse distribution parameter. Hence substituting $U_{gj} = 0$ in Equation (1), we can relate the two as follows: $\varepsilon_{drift-flux} = \varepsilon_h \cdot \frac{1}{C_o}$. This means that in annular flow, the drift flux void fraction is always less than that predicted by the homogeneous model by a factor at least $1/1.1$. Hence the highest drift flux void fractions are around 0.91, making it insensitive to increase in gas flow at high superficial gas velocities. Such a fact is evident in the plots shown in Figure 11 where the predicted void fractions by the drift flux model are compared with the experimental data. For all correlations surveyed, there is peaking of the predicted void fraction when the experimental values approach 0.85. Also, at these annular conditions, considerably more scattering of the data points can be observed. Hence, drift flux relationships should be used with caution in the annular flow regime. Conversely, good performance is obtained for bubbly flows as shown in Figure 11 (b) for the correlation of Sun [47] where most predictions are within the ±30% error margin. Drift correlations generally have a simple structure, and demonstrate good accuracy across pipe scales.

Figure 11: Comparison of large-diameter void fractions with published drift-flux-type correlations

The last category of void correlations considered is for those termed "general". Here, the void fraction is correlated with dimensionless numbers mainly the Reynolds, Froude, Weber numbers as well as the Martinelli flow parameter. Many of these correlations have been derived and take different forms with varying degrees of difficulty involved in their application. These have been summarised elsewhere [26]. While the correlations of Stearman [48] (steam-water, 1.72-18.7 MPa), and Flanigan [49] are simple in form and application in that they only require the fluid properties and superficial velocities, others are more intricate. That of Wallis [50] is simple in form but requires the evaluation of the Martinelli parameter X which involves estimating single phase pressure drops, and selecting flow regime dependent parameters. Even more complicated are those of Beggs [51], and Mukherjee [52] where pipe inclination and evaluation of complex polynomial functions are involved.

Figure 12 shows the comparison between a selection of general correlations for void fraction and the large pipe experimental data. It can be seen that their agreement with the database varies widely. The equation of Wallis [50] exhibits good performance in the bubbly and to some extent annular flow regions. However, it is in the churn and churn-turbulent regimes that large deviations occur. Coupled with the effect of pipe diameter, these flow regimes have traditionally proven difficult to model in two-phase flow. Huq and Loth's [53] equation was theoretically derived by considering the onset of boiling in vertical pipes at BWR conditions. They showed that their model agreed with the air–water data of [54] at atmospheric pressure covering a wide range of mass fluxes in a 12.25 mm vertical pipe. But it only shows excellent agreement with some of the large pipe data in the annular regime as shown in Figure 12 (b) and other predictions are mostly outside the ±30% error margin (see Table 3). The other correlations [49], [55], [56], [57], all combinations of different dimensionless numbers, produce lesser agreement with the experimental data especially at the higher gas flows. This may be due to the media used in their experiments. For example El-Boher's [56] experiments were conducted using air–liquid metal fluid combinations.

Figure 12: Comparison of large-diameter void fractions with published general correlations

In light of the relative success of the drift flux models in predicting void fractions, we found that a small adjustment of the coefficients results in a good fit to the collected database. A drift velocity defined as $U_{gj} = 0.35(\sigma g \Delta\rho/\rho_l^2)^{0.5}$ as well as the constant 1.03 which is akin to distribution parameter C_o in Equation (1) produces a correlation that is in good agreement with the data as follows:

$$\varepsilon = u_{sg} \Big/ \left[1.028\, u_{mix} + 0.35 \left(\frac{g\sigma\Delta\rho}{\rho_l^2} \right)^{0.5} \right] \quad \textbf{(6)}$$

The number 1.028 is not far from the 1.1 to 1.2 frequently encountered in the literature [18], [27] as given in Table 1. Equation (6) is valid for gas–liquid flow in vertical pipes where the dimensionless hydraulic diameter $D^* \equiv D/\sqrt{\sigma/g(\rho_l - \rho_g)}$ is between 37 and 75 corresponding to the pipe size range of 101.6–203 mm used in this study. It should be used with caution where fluids different from the air and water in the current database are involved.

Figure 13: Comparison of present correlation with the combined experimental data

Figure 14 shows that Equation (6) produces small scatter as only five data points out of a total of 347 are outside the defined ±30% error region. Therefore, the present correlation gives a mean absolute error of 15% with 98% predictions within ±30% of the experimental data. Comparing these with that produced with the previous correlations as given in Table 1, shows good performance across flow regimes, as only a few of the tested correlations produced similar agreement with the experiments [58], [50], [59], [47] [60]. These are mostly of the drift flux category as well as the homogeneous model.

Figure 14: Simulation of present correlation showing effect of gas and liquid superficial velocities

Figure 14 depicts simulated void fraction values against u_{sg} using the present correlation with each curve representing the different u_{sl} values. It exhibits the trends obtained in the experimental results as presented in Figure 6, thereby showing the ability of the correlation to adjust to test conditions including pressure/density changes which are partly implicit in the gas superficial velocity.

Table 1: Statistical performance of the various correlations against the experimental database

4 Conclusions

A capacitance wire mesh sensor was used to explore the effect of 180º bend on gas-liquid flow behaviours in the upward direction in a vertical serpentine large-diameter pipeline. Velocities used throughout this study ranged from 0.14 to 29.83 m/s for the air, and 0.07 to 1.5 m/s for water. The following conclusions are drawn from the obtained data:

1. The return bend has a substantial influence on the downstream up-flow behaviour, causing large flow misdistribution, affecting the occurrence of flow regimes, and delaying axial flow development. These were observed using reconstructed images and videos obtained from the

WMS, and in some cases, local dry spots were created due to centrifugal action occasioned by the bend.

2. Time, and cross-sectionally averaged void fraction values were observed to increase with increasing the superficial gas velocity, at all positions of the upward section. Conversely, they decreased with increasing superficial liquid velocity.
3. There is declining impact of the return bend along the pipe axis, as the flow develops. In fact, significant differences in the void fraction were observed at the bottom and top positions. However, probability density functions of the void fraction measurements at the middle and top positions were similar as well as time-averaged values, meaning that flow development is high on getting to L/D = 28. This is especially so at high gas velocities.
4. Mean void fraction measurements from this study were similar to those obtained from previous studies in large-diameter pipes, especially in the annular flow region. Also, the use of drift flux models to predict the void fraction produces the best performance against other model categories. A drift-flux type correlation was obtained that better describes the database collected for this study.

Acknowledgement

AAA received funding for his PhD from the Libyan Government and is deeply grateful. AMA received funding from the Nigerian Government for funding his PhD through the Petroleum Technology Development Fund's Overseas Scholarship Scheme (PTDF/E/OSS/PHD/AMA/622/12). The authors also acknowledge the courtesy WMS spool, data processing and image reconstruction software, and technical support to this study, by Prof. Hampel and his group at Helmholtz-Zentrum Dresden-Rossendorf, Germany, and by Prof. Da Silva and his group at Universidade Tecnológica Federal do Paraná, Brazil.

Conflict of Interest

None declared.

References

[1] G. E. Alves, "Co-current liquid-gas flow in a pipe-line contactor," *Chem. Eng. Prog.*, vol. 50, no. 9, pp. 449–456, 1954.

[2] T. Oshinowo and M. E. Charles, "Vertical two-phase flow part I. Flow pattern correlations," *Can. J. Chem. Eng.*, vol. 52, no. 1, pp. 25–35, Feb. 1974.

[3] G. H. Anderson and P. D. Hills, "Two-phase annular flow in tube bends," in *Symposium on Multiphase Flow Systems*, 1974.

[4] K. Usui, S. Aoki, and A. Inoue, "Flow Behavior and Phase Distribution in Two-Phase

563 Flow around Inverted U-Bend," *J. Nucl. Sci. Technol.*, vol. 20, no. 11, pp. 915–928,
564 1983.
565 [5] T. Takemura, K. Roko, M. Shiraha, and S. Midoriyama, "Dryout characteristics and
566 flow behavior of gas-water two-phase flow through U-shaped and inverted U-shaped
567 bends," *Nucl. Eng. Des.*, vol. 95, pp. 365–373, 1986.
568 [6] B. Poulson, "Measuring and modelling mass transfer at bends in annular two phase
569 flow," *Chem. Eng. Sci.*, vol. 46, no. 4, pp. 1069–1082, 1991.
570 [7] A. M. Ribeiro, T. R. Bott, and D. M. Jepson, "The influence of a bend on drop sizes in
571 horizontal annular two-phase flow," 2001.
572 [8] A. Azzi and L. Friedel, "Two-phase upward flow 90 degree bend pressure loss model,"
573 *Forsch. im Ingenieurwes.*, pp. 120–130, 2005.
574 [9] K. Hoang and M. R. Davis, "Flow Structure and Pressure Loss for Two Phase Flow in
575 Return Bends," *J. Fluids Eng.*, vol. 106, no. 1, pp. 30–37, Mar. 1984.
576 [10] P. W. James, B. J. Azzopardi, D. I. Graham, and C. A. Sudlow, "The effect of a bend on
577 droplet distribution in two-phase flow," in *International Conference on Multiphase*
578 *Flow in Industrial Plants*, 2000.
579 [11] L. Y. Chong, B. J. Azzopardi, and D. J. Bate, "Calculation of Conditions at Which
580 Dryout Occurs in the Serpentine Channels of Fired Reboilers," *Chem. Eng. Res. Des.*,
581 vol. 83, no. 4, pp. 412–422, 2005.
582 [12] B. J. Azzopardi, "Drops in annular two-phase flow," *Int. J. Multiph. Flow*, vol. 23, no.
583 7, pp. 1–53, 1997.
584 [13] J. D. Balfour and D. L. Pearce, "Annular flows in horizontal 180o bends: Measurements
585 of water rate distributions in the film and vapour Core," 1978.
586 [14] P. Domanski and C. Hermes, "An improved two-phase pressure drop correlation for
587 180° return bends," in *3rd Asian Conference on Refrigeration*, 2006, pp. 21–24.
588 [15] M. Sharma, P. Ravi, S. Ghosh, G. Das, and P. K. Das, "Hydrodynamics of lube oil-water
589 flow through 180?? return bends," *Chem. Eng. Sci.*, vol. 66, no. 20, pp. 4468–4476,
590 2011.
591 [16] M. Abdulkadir, D. Zhao, A. Azzi, I. S. Lowndes, and B. J. Azzopardi, "Two-phase air-
592 water flow through a large diameter vertical 180 o return bend," *Chem. Eng. Sci.*, vol.
593 79, pp. 138–152, 2012.
594 [17] P. D. Hills, "A study of two-phase (gas-liquid) flow in a tube bend," Imperial College,
595 London, 1973.

[18] I. Kataoka and M. Ishii, “Drift flux model for large diameter pipe and new correlation for pool void fraction,” *Int. J. Heat Mass Transf.*, vol. 30, no. 9, pp. 1927–1939, Sep. 1987.

[19] H. Cheng, J. H. Hills, and B. J. Azzorpardi, “A study of the bubble-to-slug transition in vertical gas-liquid flow in columns of different diameter,” *Int. J. Multiph. Flow*, vol. 24, no. 3, pp. 431–452, 1998.

[20] A. Ohnuki and H. Akimoto, “Experimental study on transition of flow pattern and phase distribution in upward air–water two-phase flow along a large vertical pipe,” *Int. J. Multiph. Flow*, vol. 26, no. 3, pp. 367–386, 2000.

[21] J. P. Schlegel, P. Sawant, S. Paranjape, B. Ozar, T. Hibiki, and M. Ishii, “Void fraction and flow regime in adiabatic upward two-phase flow in large diameter vertical pipes,” *Nucl. Eng. Des.*, vol. 239, no. 12, pp. 2864–2874, 2009.

[22] S. F. Ali, “Two-phase flow in a large diameter vertical riser,” Cranfield University, 2009.

[23] J. P. Schlegel, S. Miwa, S. Chen, T. Hibiki, and M. Ishii, “Experimental study of two-phase flow structure in large diameter pipes,” *Exp. Therm. Fluid Sci.*, vol. 41, no. 2012, pp. 12–22, Sep. 2012.

[24] V. M. Alipchenkov, R. I. Nigmatulin, S. L. Soloviev, O. G. Stonik, L. I. Zaichik, and Y. A. Zeigarnik, “A three-fluid model of two-phase dispersed-annular flow,” *Int. J. Heat Mass Transf.*, vol. 47, no. 24, pp. 5323–5338, 2004.

[25] V. Stevanovic, S. Prica, and B. Maslovaric, “Multi-Fluid Model Predictions of Gas-Liquid Two-Phase Flows in Vertical Tubes,” *FME Trans.*, vol. 35, pp. 173–181, 2007.

[26] M. A. Woldesemayat and A. J. Ghajar, “Comparison of void fraction correlations for different flow patterns in horizontal and upward inclined pipes,” *Int. J. Multiph. Flow*, vol. 33, no. 4, pp. 347–370, 2007.

[27] T. Hibiki and M. Ishii, “One-dimensional drift – flux model for two-phase flow in a large diameter pipe,” *Int. J. Heat Mass Transf.*, vol. 46, pp. 1773–1790, 2003.

[28] M. H. S. Zangana, “Film behaviour of vertical gas-Liquid Flow in a large diameter pipe,” University of Nottingham, 2011.

[29] G. P. Van der Meulen, “Churn-Annular Gas-Liquid Flows in Large Diameter Vertical Pipes,” PhD Thesis, University of Notingham, 2012.

[30] A. Skopich, E. Pereyra, C. Sarica, and M. Kelkar, “Pipe-diameter effect on liquid loading in vertical gas wells,” *SPE Prod. Oper.*, vol. 30, no. 2, pp. 164–176, 2015.

[31] M. J. Da Silva, E. Schleicher, and U. Hampel, “Capacitance wire-mesh sensor for fast measurement of phase fraction distributions,” *Meas. Sci. Technol. Meas. Sci. Technol*, vol. 18, no. 18, pp. 2245–2251, 2007.

[32] A. A. Almabrok, “Gas-Liquid two-phase flow in up and down vertical pipes,” Cranfield University, 2014.

[33] A. A. Almabrok, A. M. Aliyu, L. Lao, and H. Yeung, “Gas/liquid flow behaviours in a downward section of large diameter vertical serpentine pipes,” *Int. J. Multiph. Flow*, vol. 78, pp. 25–43, 2016.

[34] D. J. Peng, M. Ahmad, C. P. Hale, O. K. Matar, and G. F. Hewitt, “Flow regime transitions in large diameter pipes,” in *7th International Conference on Multiphase Flow (Multiphase 7)*, 2010, pp. 1–9.

[35] L. Lao, L. Xing, and H. Yeung, “Behaviours of elongated bubbles in a large diameter riser,” in *8th North American Conference on Multiphase Technology (Multiphase 8)*, 2012, no. 1998, pp. 381–392.

[36] B. J. Azzopardi and E. Wren, “What is entrainment in vertical two-phase churn flow?,” *Int. J. Multiph. Flow*, vol. 30, no. 1, pp. 89–103, 2004.

[37] Y. Taitel, D. Bornea, and A. E. Dukler, “Modelling flow pattern transitions for steady upward gas-liquid flow in vertical tubes,” *AIChE J.*, vol. 26, no. 3, pp. 345–354, May 1980.

[38] N. K. Omebere-Iyari and B. J. Azzopardi, “A Study of Flow Patterns for Gas/Liquid Flow in Small Diameter Tubes,” *Chem. Eng. Res. Des.*, vol. 85, no. 2, pp. 180–192, 2007.

[39] M. Abdulkadir, “Experimental and computational fluid dynamics (CFD) studies of gas-liquid flow in bends,” University of Nottingham, UK, 2011.

[40] N. K. Omebere-Iyari, “The effect of pipe diameter and pressure in vertical two-phase flow,” University of Nottingham, 2006.

[41] R. W. Lockhart and R. c. Martinelli, “Proposed correlation of data for isothermal two-phase, two-component flow in pipes,” *Chemecal Engineering Progress*, vol. 45, no. 1. pp. 39–48, 1949.

[42] D. Chisholm, “Pressure gradients due to friction during the flow of evaporating two-phase mixtures in smooth tubes and channels,” *Int. J. Heat Mass Transf.*, vol. 16, no. 2, pp. 347–358, 1973.

[43] J. M. Turner and G. B. Wallis, “The separate-cylinders model of two-phase flow,” 1965,

662 p. Paper No. NYO-3114-6.
663 [44] S. G. Bankoff, “A Variable Density Single-Fluid Model for Two-Phase Flow With
664 Particular Reference to Steam-Water Flow,” *J. Heat Transfer*, vol. 82, no. 4, p. 265,
665 1960.
666 [45] D. J. Nicklin, “Two-phase bubble flow,” *Chem. Eng. Sci.*, vol. 17, no. 9, pp. 693–702,
667 Sep. 1962.
668 [46] N. Zuber and J. A. Findlay, “Average Volumetric Concentration in Two-Phase Flow
669 Systems,” *J. Heat Transfer*, vol. 87, no. 4, pp. 453–468, Nov. 1965.
670 [47] K. H. Sun, R. B. Duffey, and C. M. Peng, “Thermal-hydraulic analysis of core
671 unrecovery,” in *Proceedings of the 19th National Heat Transfer Conference,*
672 *Experimental and Analytical Modeling of LWR Safety Experiments*, 1980, pp. 1–10.
673 [48] L. S. Stearman, “The generalization of experimental data concerning the bubbling of
674 vapor through liquid,” *J. Tech. Phys.*, vol. 26, no. 1519, 1956.
675 [49] O. Flanigan, “Effect of uphill flow on pressure drop in design of two-phase gathering
676 systems,” *Oil Gas J.*, vol. 56, pp. 132–141, 1958.
677 [50] G. B. Wallis, *One Dimensional Two-Phase Flow*, vol. null. New York: McGraw-Hill,
678 1969.
679 [51] H. D. Beggs, “An experimental study of two phase flow in inclined pipes,” The
680 University of Tulsa, Tulsa, OK, USA, 1972.
681 [52] H. Mukherjee, “An experimental study of inclined two-phase flow,” The University of
682 Tulsa, Tulsa, OK, USA, 1979.
683 [53] R. Huq and J. L. Loth, “Analytical two-phase flow void prediction method,” *J.*
684 *Thermophys. Heat Transf.*, vol. 6, no. 1, pp. 139–144, Jan. 1992.
685 [54] G. H. Anderson and B. G. Mantzouranis, “Two-phase (gas/liquid) flow phenomena—
686 II: Liquid entrainment,” *Chem. Eng. Sci.*, vol. 12, no. 4, pp. 233–242, 1960.
687 [55] L. G. Neal and S. G. Bankoff, “Local parameters in cocurrent mercury-nitrogen flow:
688 Parts I and II,” *AIChE J.*, vol. 11, no. 4, pp. 624–635, Jul. 1965.
689 [56] A. El-Boher, S. Lesin, Y. Unger, and H. Branover, “Experimental studies of two phase
690 liquid metal gas flows in vertical pipes,” in *Proceedings of the 1st World conference on*
691 *Experimental Heat Transfer*, 1988.
692 [57] D. A. Yashar, M. J. Wilson, H. R. Kopke, D. M. Graham, J. C. Chato, and T. A. Newell,
693 “An investigation of refrigerant void fraction in horizontal, microfin tubes,” *ASHRAE*
694 *Trans.*, vol. 107 PART 2, no. January 2015, pp. 173–188, 2001.

[58] G. a. Hughmark, “Holdup and heat transfer in horizontal slug gas-liquid flow,” *Chem. Eng. Sci.*, vol. 20, no. 12, pp. 1007–1010, 1965.

[59] Gregory and Scott, “Correlation of Liquid Slug Velocity and Frequency in Horizontal Cocurrent Gas-Liquid Slug Flow,” *AIChE J.*, vol. 15, no. 6, pp. 933–935, 1969.

[60] S. Morooka, T. Ishizuka, M. Iizuka, and K. Yoshimura, “Experimental study on void fraction in a simulated BWR fuel assembly (evaluation of cross-sectional averaged void fraction),” *Nucl. Eng. Des.*, vol. 114, no. 1, pp. 91–98, May 1989.

[61] D. Chisholm, *Two-phase flow in pipelines and heat exchangers*. G. Godwin in association with Institution of Chemical Engineers, 1983.

[62] G. E. Dix, “Vapor void fractions for forced convection with subcooled boiling at low flow rates.,” 1971.

Figures

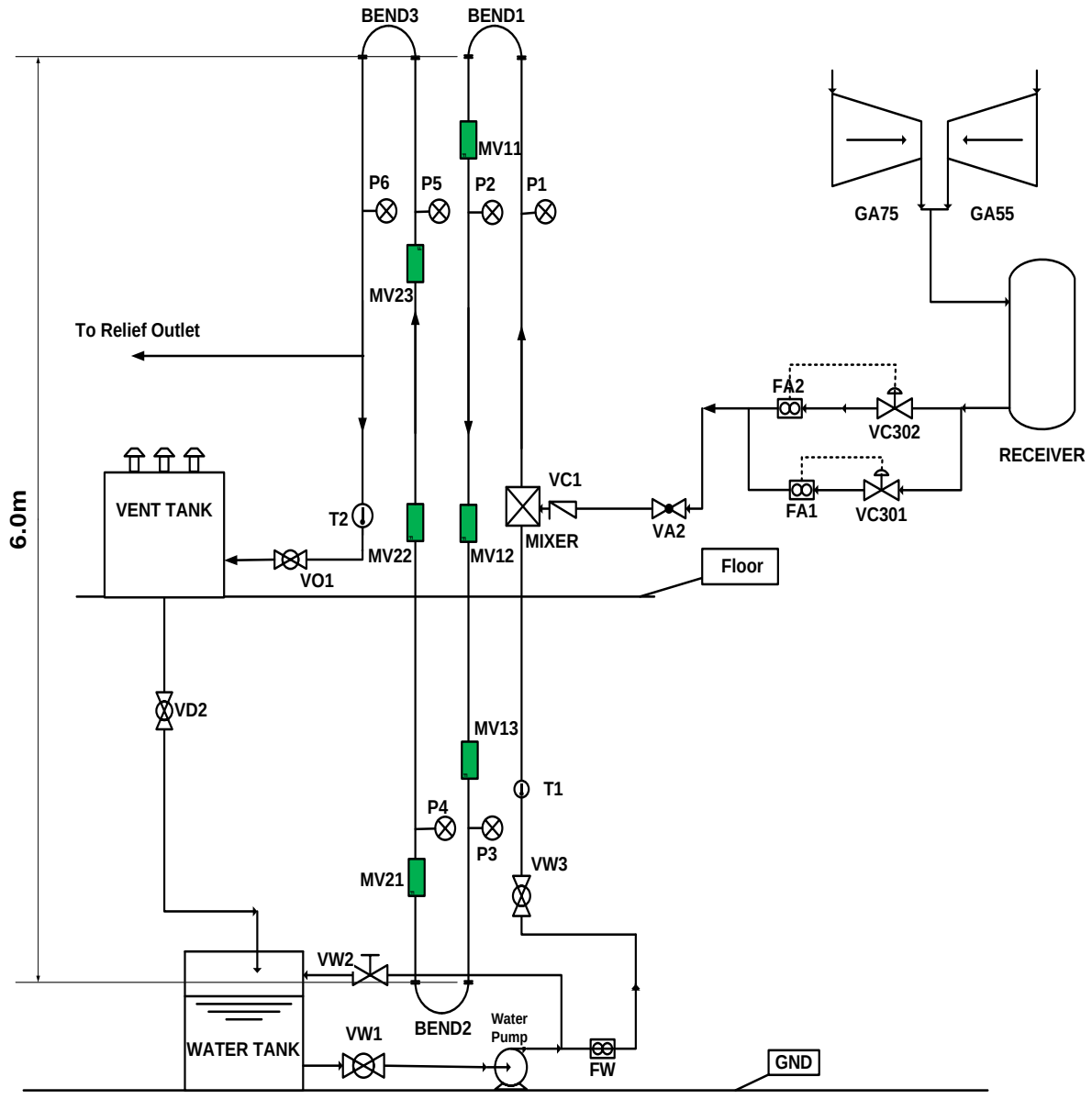

Figure 1: Schematic of the Serpent rig. Location of WMS is at MV21, MV22 and MV23 corresponding to L/D = 5, 28 and 47 respectively.

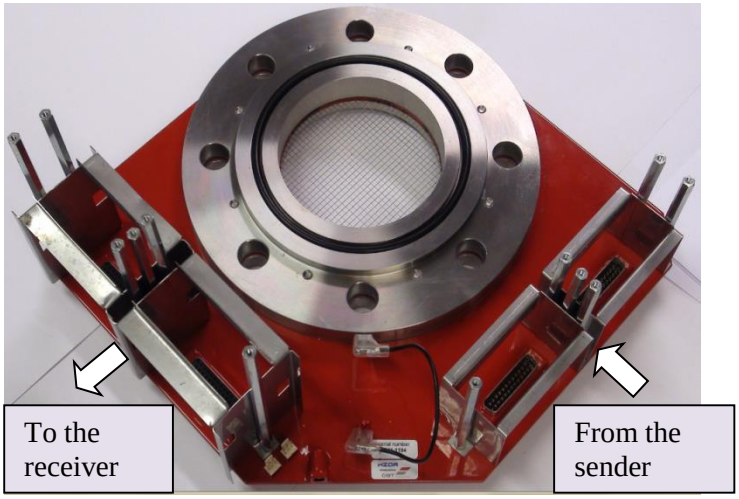

(a)

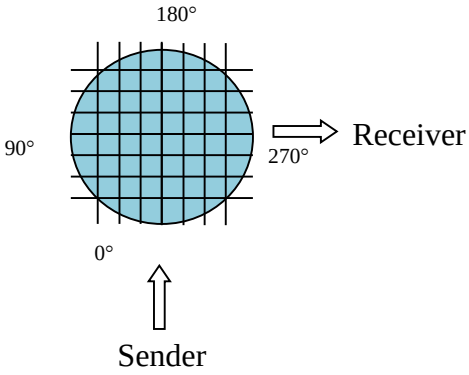

(b)

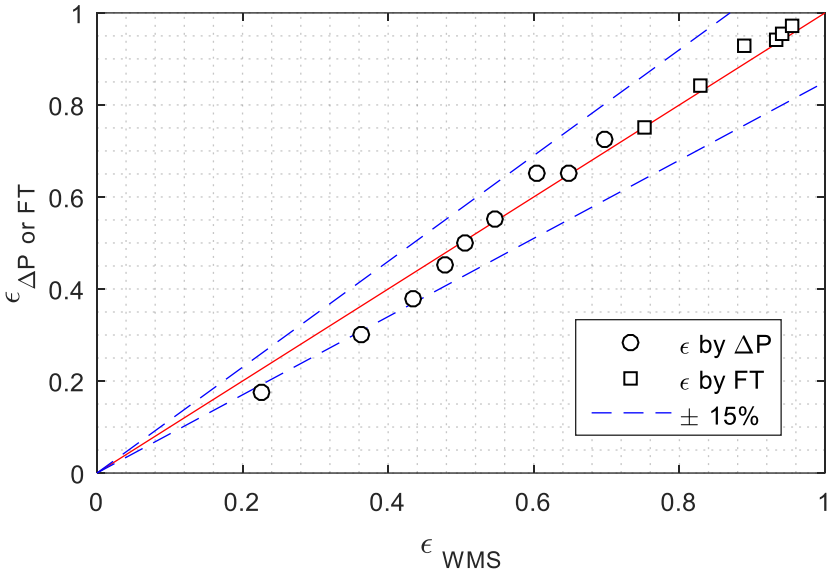

(c)

Figure 2: (a) WMS (b) its cross-sectional orientation (c) validation of WMS void fraction with those obtained by ΔP and film thickness (FT) measurements at $u_{sl} = 0.2$ m/s

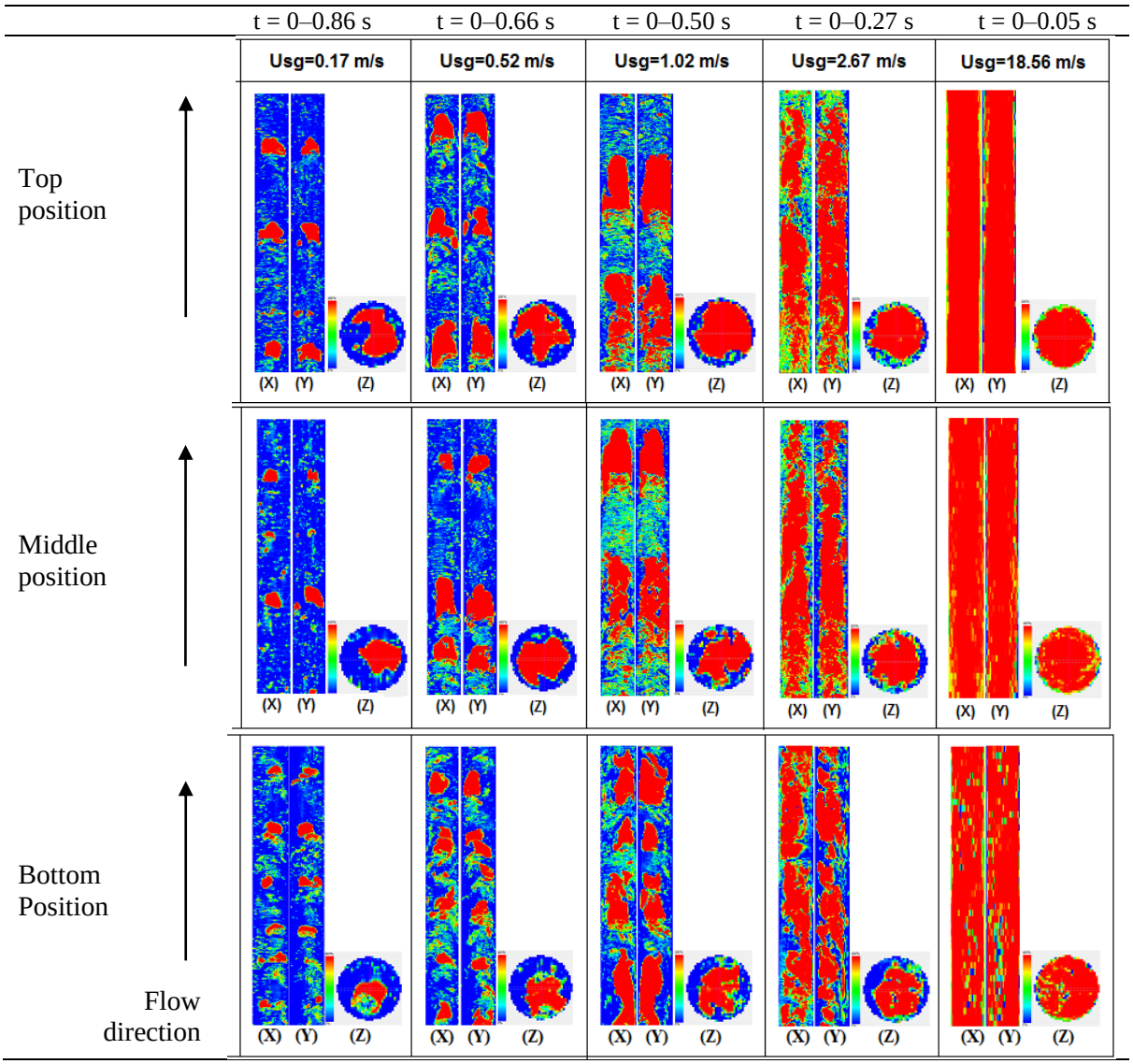

Figure 3: Reconstructed images of the phase distributions at different locations along the upward section for different superficial air velocities (u_{sg}) and a fixed superficial water velocity (u_{sl}) of 1 m/s (X and Y are representing the axial slice images, and Z is representing the cross section images . For all images the red colour is air and the blue colour is water).

u_{sg} = 0.17 m/s	u_{sg} = 0.52 m/s	u_{sg} = 1.02 m/s	u_{sg} = 2.67 m/s	u_{sg} = 18.56 m/s
Top position				
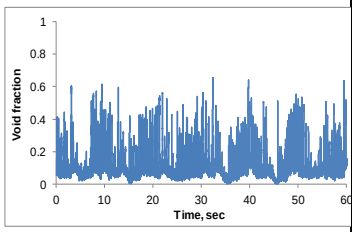	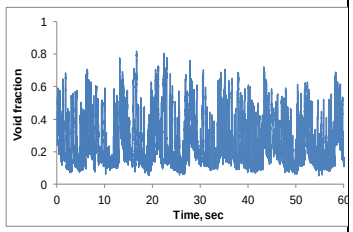	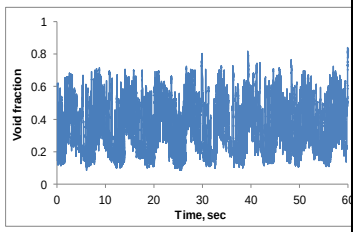	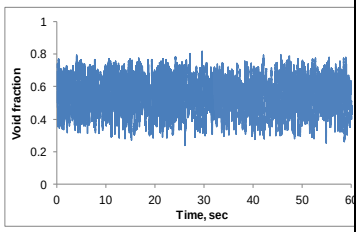	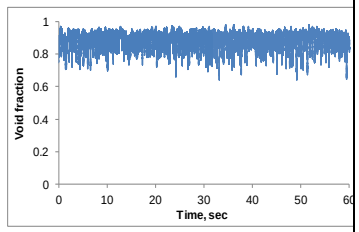
Middle position				

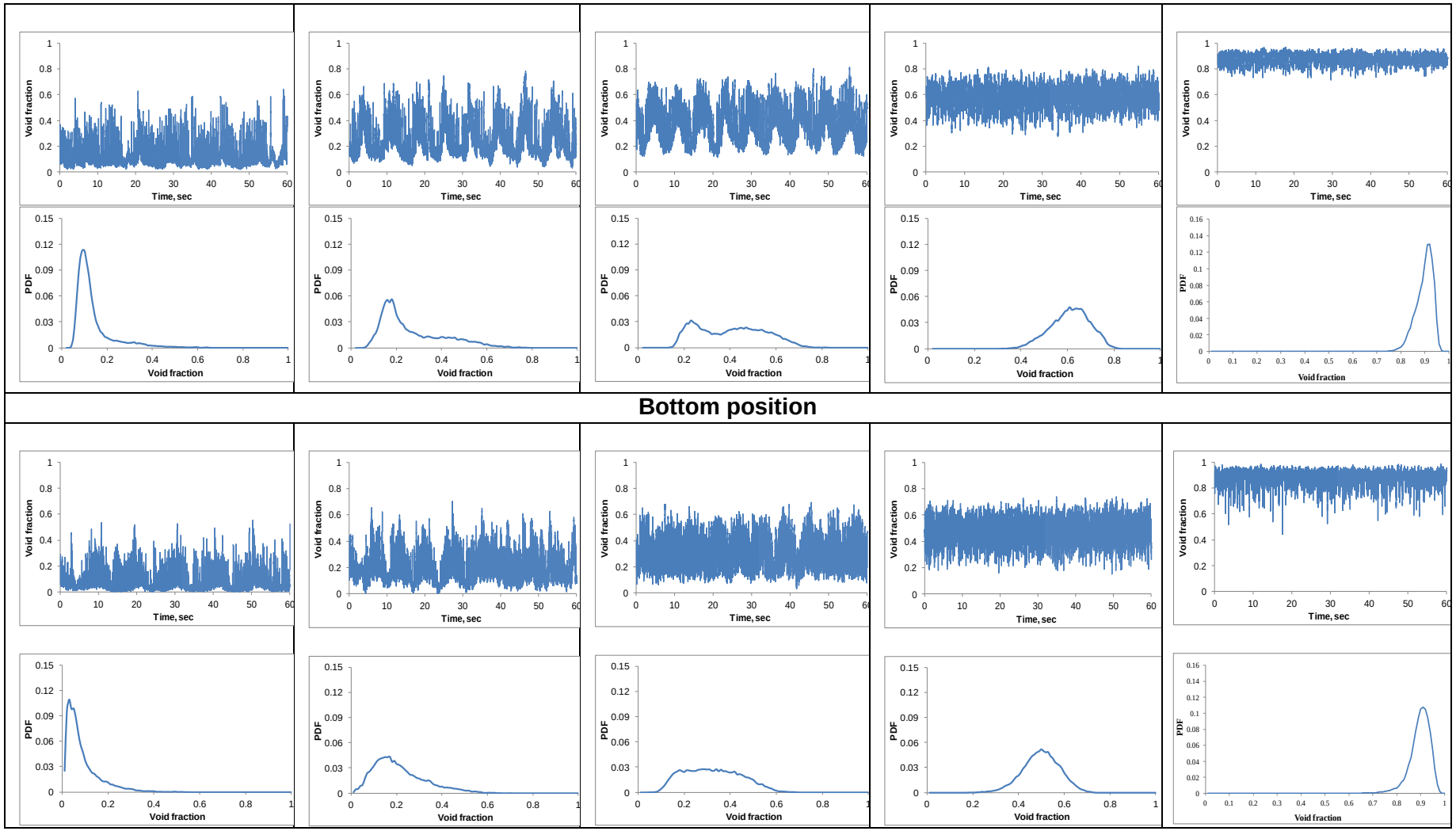

Figure 4: Time traces and their PDFs of the void fraction, respectively at the top, middle and bottom positions of upward section at different superficial air velocities (u_{sg}) and a fixed superficial water velocity (u_{sl}) of 1.0 m/s.

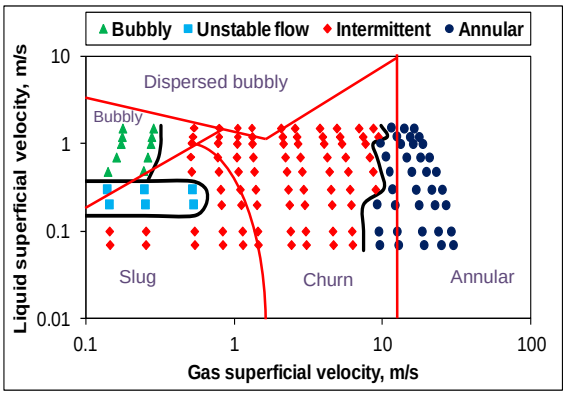

(a) Top position

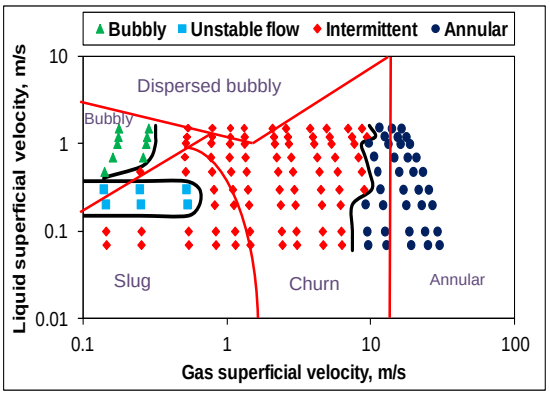

(b) Middle position

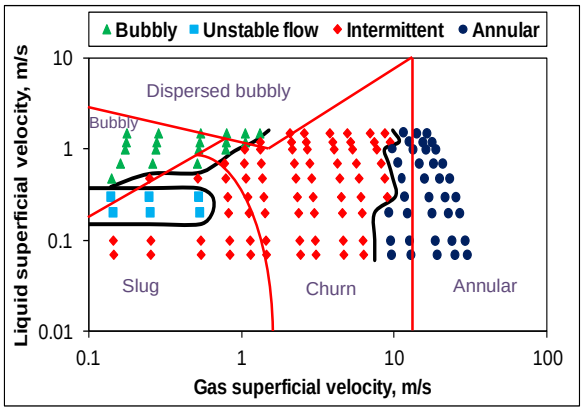

(c) Bottom position

Figure 5: Flow regime maps at the top, middle and bottom positions of upward section, respectively of this study compared with the up-flow regime map reported by Taitel et al. [32] (red lines and text) in 51 mm pipe diameter.

2

3

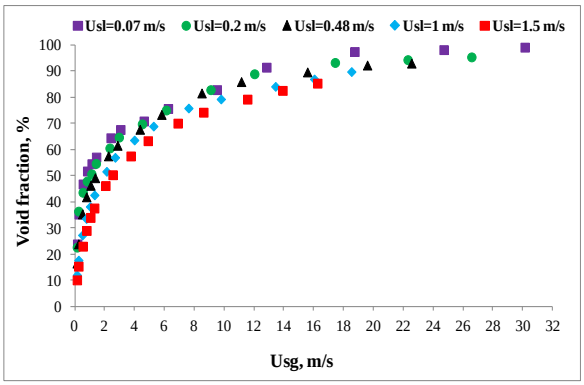

(a) Top position

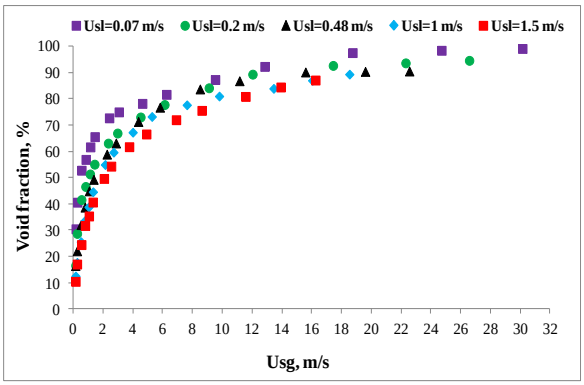

(b) Middle position

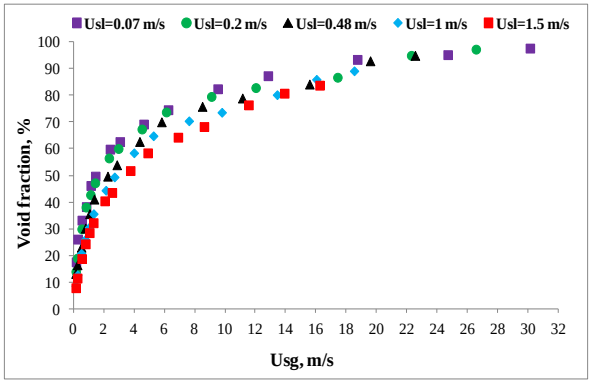

(c) Bottom position

Figure 6: The effect of the superficial air velocities (u_{sg}) and superficial water velocities (u_{sl}) on the void fraction development at the top, middle and bottom positions of the upward section (P = 0.9–1.3 bar).

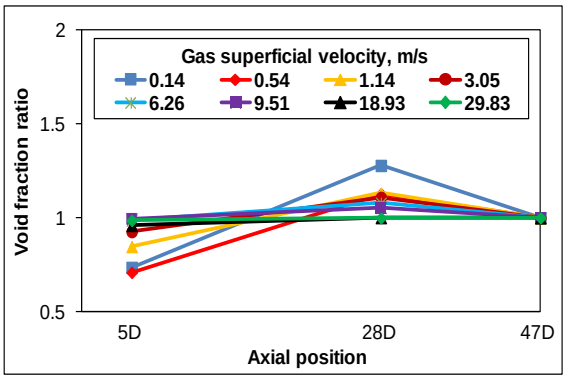

(a) u_{sl} = 0.07 m/s

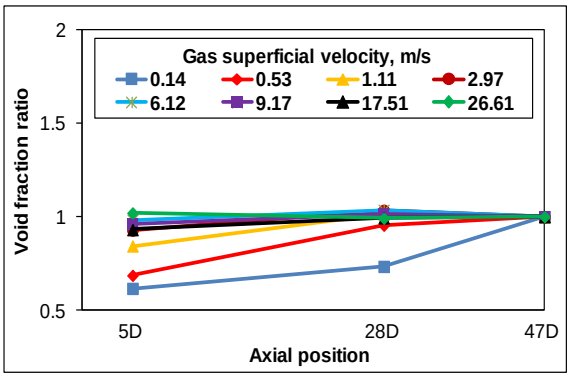

(b) u_{sl} = 0.2 m/s

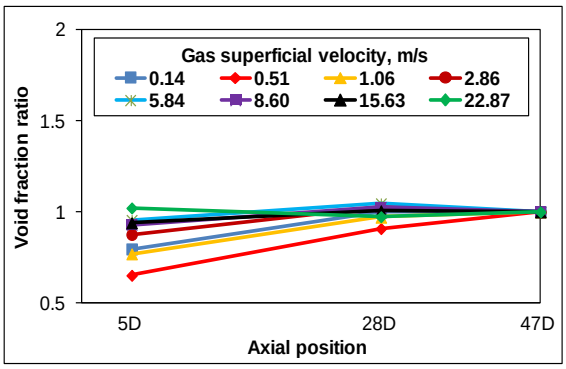

(c) u_{sl} = 0.48 m/s

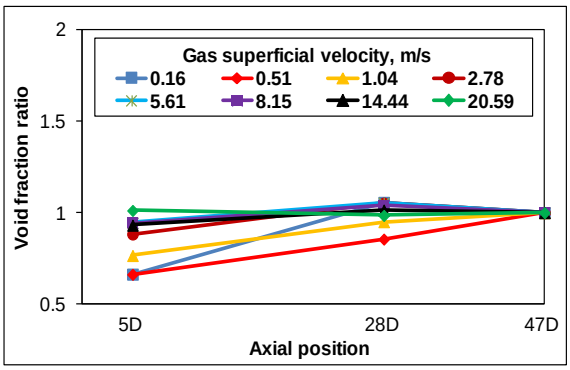

(d) u_{sl} = 0.7 m/s

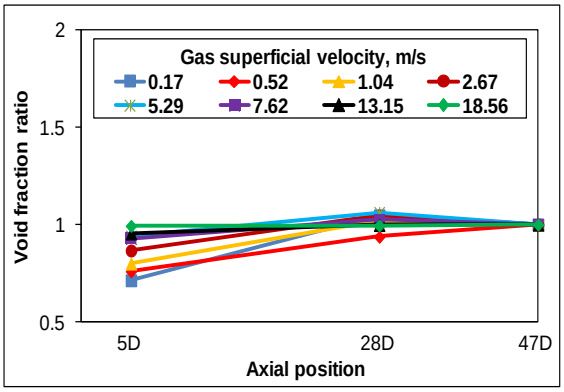

(e) u_{sl} = 1.0 m/s

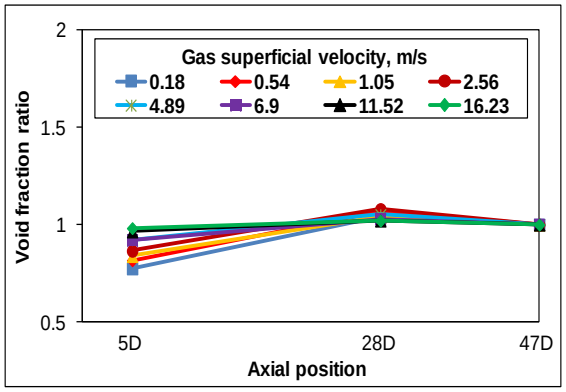

(f) u_{sl} = 1.5 m/s

Figure 7: Void fraction variations along upward section.

u_{sg} =0.17 m/s	u_{sg} =0.52 m/s	u_{sg} =9.65 m/s

Top position

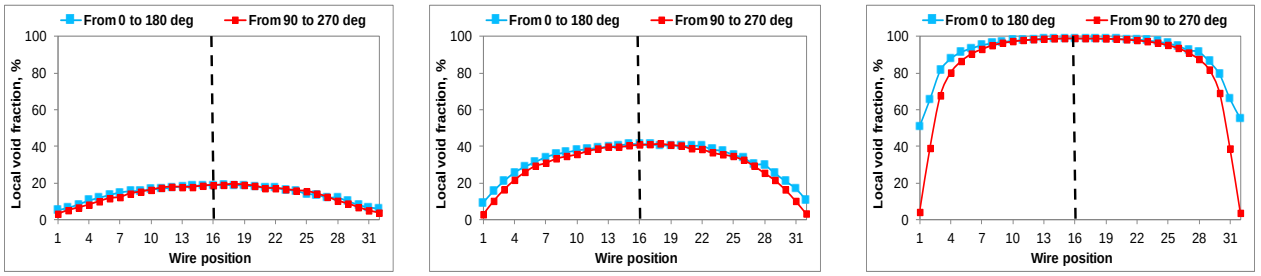

Middle position

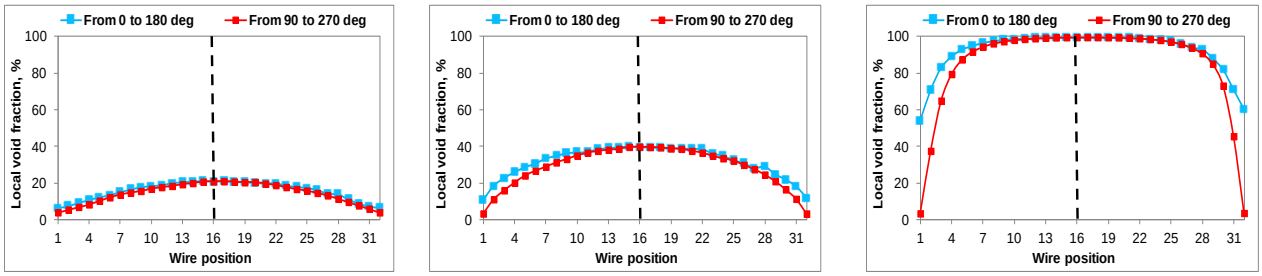

Bottom position

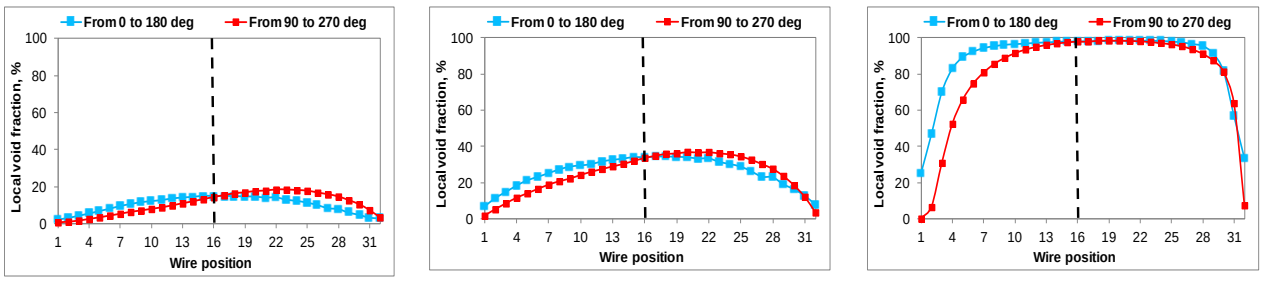

Figure 8: Chordal distributions of the void fraction at the top, middle and bottom positions of upward section, for different superficial air velocities (u_{sg}) and a fixed superficial water velocity (u_{sl}) of 1.0 m/s.

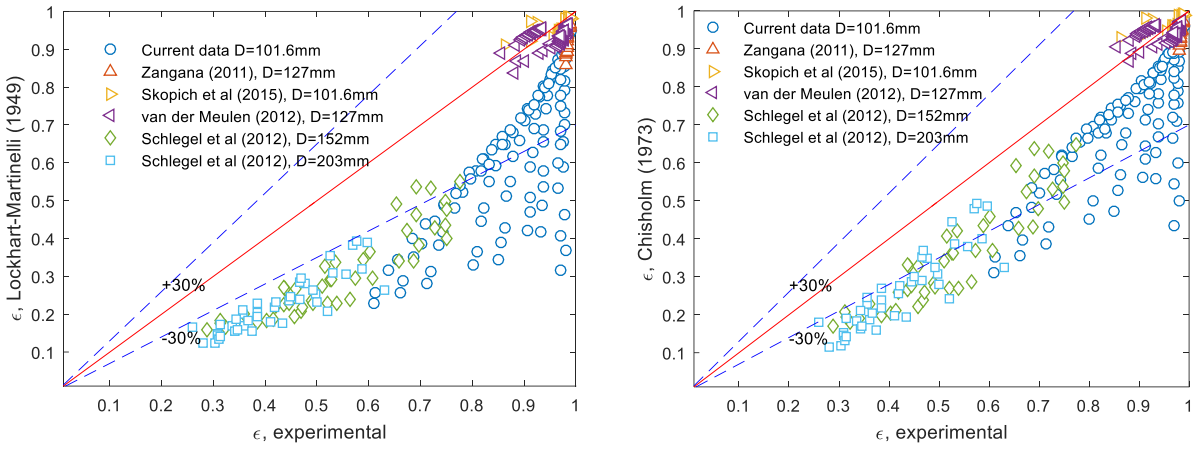

12 **Figure 9: Comparison of large diameter void fractions with published slip ratio-type correlations**

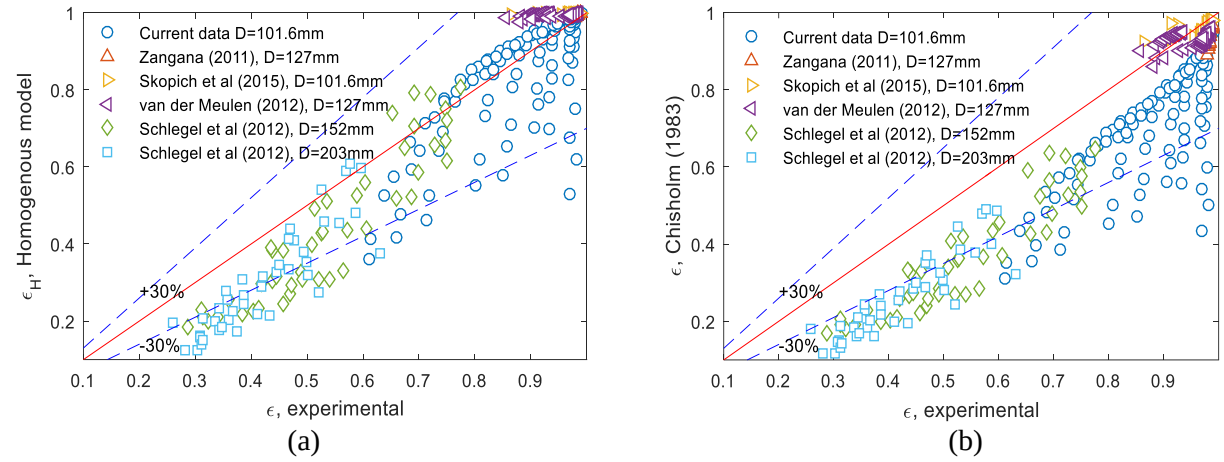

13 **Figure 10: Comparison of large diameter void fractions with published no-slip-type correlations**

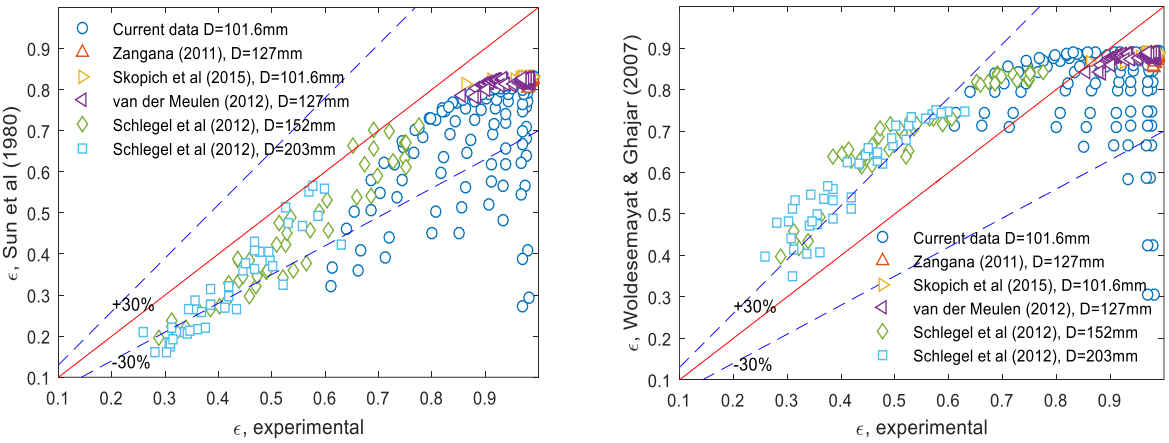

14 **Figure 11: Comparison of large diameter void fractions with published drift-flux-type correlations**

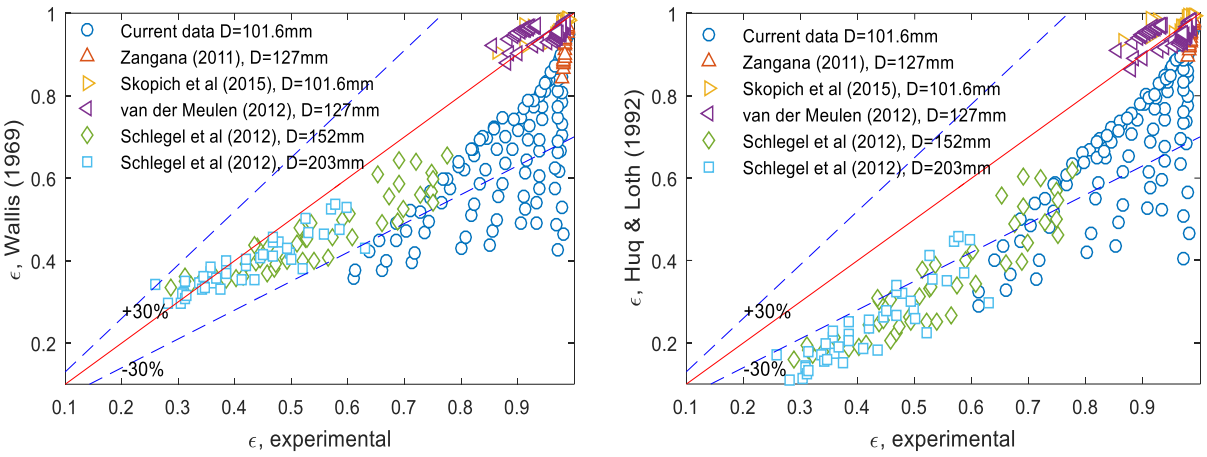

(a) (b)

Figure 12: Comparison of large diameter void fractions with published general correlations

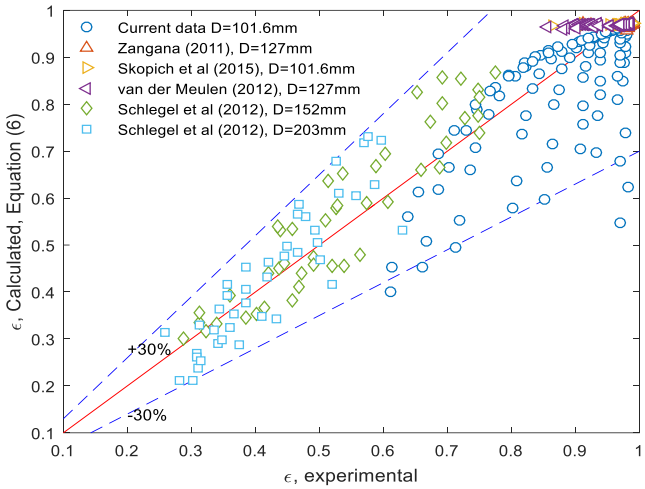

Figure 13: Comparison of present correlation with the combined experimental data

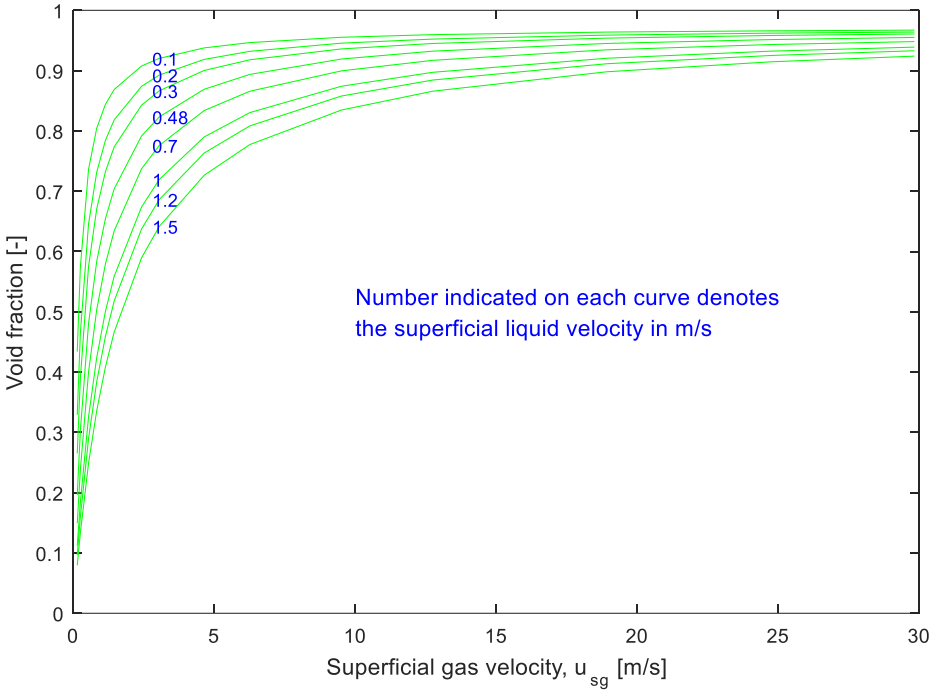

Figure 14: Simulation of present correlation showing effect of gas and liquid superficial velocities

Tables

Table 1: Selected void fraction correlations

Lockhart and Martinelli [31]	$\varepsilon = 1/\left[1 + 0.28\left(\frac{1-x}{x}\right)^{0.64}\left(\frac{\rho_g}{\rho_l}\right)^{0.36}\left(\frac{\mu_g}{\mu_l}\right)^{0.07}\right]$	One of the most famous and robust empirical relationships for two-phase void fraction and pressure drop. Liquids used in combination with air are: benzene, water, kerosene, and various oils. Pipe diameters range between 1.5–25 mm in diameter. Introduced the use of the dimensionless parameter *X*.
Wallis [32]	$\varepsilon = [1 + X_{tt}^{0.8}]^{-0.38}$	Theoretical model
Chisholm [33]	$\varepsilon = 1/\left\{1 + \left[1 - x\left(1 - \frac{\rho_l}{\rho_g}\right)\right]^{0.5}\left(\frac{1-x}{x}\right)\left(\frac{\rho_g}{\rho_l}\right)\right\}$	Theoretical.
Sun et al. [34]	$\varepsilon = \mathrm{u}_{sg}/\left\{\frac{u_{mix}}{\left[0.82+0.18\frac{P}{P_c}\right]} + 1.41\left(\frac{g\sigma\Delta\rho}{\rho_l^2}\right)^{0.25}\right\}$	Semi-empirical. Theoretical arguments were combined with the drift-flux correlation of Dix.
Chisholm [35]	$\varepsilon = \varepsilon_h/\left[\varepsilon_h + \sqrt{1-\varepsilon_h}\right]$	Theoretical, tested against data collected from pipes and the shell side of horizontal heat exchangers
Huq and Loth [36]	$\varepsilon = 1 - \frac{2(1-2x)^2}{1-2x+\sqrt{1+4x(1-x)\left(\frac{\rho_l}{\rho_g}-1\right)}}$	Analytical, derived to predict lower limit of void fraction in terms of gas quality and system pressure, using functions of the slip and boundary conditions for minimum and maximum *x*.
Woldesemayat and Ghajar [26]	$\varepsilon = \frac{\mathrm{u}_{sg}}{\left\{\mathrm{u}_{sg}\left[1+\left(\frac{u_{sg}}{u_{sl}}\right)\left(\frac{\rho_g}{\rho_l}\right)^{0.1}\right]+2.9\left[\frac{gD\sigma\Delta\rho(1+\cos\theta)}{\rho_l^2}\right]^{0.25}(1.22+1.22\sin\theta)^{\frac{P_{atm}}{P_{sys}}}\right\}}$	Used 2700 data points from various databases comprising horizontal, inclined and vertical flow, for air/water, air/kerosene mixtures. Pipe diameters ranged between 12–78 mm in diameter. Modified [37] correlation by introducing two correction factors to account for operating pressure and pipe inclination.

33 **Table 2: Available literature void fraction data for large diameter upward flow**

S/No.	Author(s)	D (mm)	L/D	Test pressure (bara)	u_{sl} range (m/s)	u_{sg} range (m/s)	Flow regime*	Number of data points
1	Zangana [28]	127	66	1.0	0.02–0.1	7.5–17	A	20
2	Van der Meulen [29]	127	87	2.0	0.014–0.04	7–16	C, A	82
3	Schlegel et al. [23]	152, 203	26, 33.9	2.0	0.4–1.0	0.2–3.2	B, CB, CT	88
4	Skopich et al. [30]	101.6	58– 92	0.9–1.2	0.01–0.05	14–27	C, A	20
5	Current	101.6	46	1.0–1.4	0.1-1.5	0.14–30	B, C, A	111
	Total							347

* A – annular, B – bubbly, C – Churn, CB – spherical cap bubbly, CT – churn–turbulent

34

35

Table 3: Statistical performance of the various correlations against the experimental database

Correlation	% MAE	% Points withn 30% of experiments
i. Slip ratio-type correlations		
Lockhart–Martinelli [31]	24.6	53.6
Chisolm [33]	17.9	68.6
ii. No-slip-type correlations		
Homogenous model	11.8	79.0
Chisolm [35]	18.2	68.6
iii. Drift-flux-type correlations		
Sun et al [34]	19.7	76.9
Woldesemayat and Ghajar [26]	17.6	73.8
iv. General correlations		
Wallis [32]	13.4	81.0
Huq and Loth [36]	19.8	63.7